ELSEVIER

Journal of Nuclear Materials 313–316 (2003) 1183–1187

journal of nuclear materials

www.elsevier.com/locate/jnucmat

Multi-dimensional impurity transport code by Monte Carlo method including gyro-orbit effects

I. Hyodo *, M. Hirano, K. Miyamoto, K. Hoshino, A. Hatayama

Faculty of Science and Technology, 3-14-1 Hiyoshi Kouhoku-ku, Keio University, Yokohama 223-8522, Japan

Abstract

We are developing a new 3D Monte Carlo transport code 'IMPGYRO' for the analysis of the heavy impurities in fusion edge plasmas. The code directory solves the 3D equations of motion for the test impurity ions to take into account their gyro motion. Most of the important processes, such as the multi-step ionization process and Coulomb scattering, etc., are also included in the model. The results for the prompt redeposition rate of tungsten ions agree well with the analytic results. In addition, 2D density profiles for tungsten ions of each charge state in a simple slab geometry have been calculated for given background plasma profiles typical of a detached plasma state. Although the code is now still under development, these initial results show that the code has potential as a useful tool, not only for the analysis of the prompt redeposition very close to the wall, but also for the analysis of more large scale impurity transport processes.

PACS: 52.40.H
Keywords: Impurity transport; Monte Carlo method; Tungsten; Sputtering; Prompt redeposition; Detached plasma

1. Introduction

In the modeling of impurity behavior, various phenomena, such as (a) impurity generation by plasma–surface interactions, (b) ionization of sputtered neutrals, (c) impurity transport, (d) Coulomb scattering and (e) multi-step ionization and recombination processes in the plasmas, have to be included in the model. Various kinds of simulation models have been developed up to now [1–8] and they have been successfully applied both to the understanding of the underlying physics and to the design activities of fusion devices.

Under relatively high particle flux and low temperature conditions in the divertor region of future fusion reactors, erosion problems will become serious for plasma facing components made of low-Z material. Under such conditions, high-Z materials, particularly tungsten, are considered to be one of the favorable candidates, mainly due to their low sputtering yield and their high threshold sputtering energy. In addition, recently, it has been pointed out that another favorable aspect of 'prompt redeposition' further reduces the net erosion rate under high-density divertor operation [9,10]. Because of short mean free path and large Larmor radius, the probability of prompt local redeposition within the first gyro motion after the ionization is high.

In order to analyze heavy metal impurities like tungsten, their gyro motion becomes relatively important and the effect has to be included in the model in addition to the guiding center motion along the field line. For this purpose, we are now developing a 3D Monte Carlo impurity transport code. The code directly solves the 3D equations of motion for impurity ions and includes most of important phenomena listed above. In the present article, we briefly summarize our simulation model and its initial results are presented.

* Corresponding author. Tel.: +81-45 566 1607; fax: +81-45 566 1587.
E-mail address: akh@ppl.appi.keio.ac.jp (I. Hyodo).

0022-3115/03/$ - see front matter
PII: S0022-3115(02)01523-4

2. Numerical model

2.1. Neutral transport

The code traces neutral impurity trajectories until they are ionized or they reach the calculation boundary. In the present study, tungsten impurity is analyzed. Only the physical sputtering is considered in the analysis. The ionization rate coefficient for tungsten is calculated from Ref. [11]. The ionized point (the ionization length $L_{\rm ion}$) is determined from $\int_0^{L_{\rm ion}} {\rm d}s/\lambda(s) = -\ln \xi_1$ by a uniform random number ξ_1 ($0 < \xi_1 \leqslant 1$). The calculation domain is divided into small cells and background plasma profiles are specified to calculate the local mean free path $\lambda(s)$ along the trajectory. A test flight is launched from a given initial point according to an impurity source profile with a given velocity. The neutral density in each numerical cell is obtained from a path length estimator method as described in Ref. [12].

2.2. Impurity ion transport

Most of the existing impurity transport codes use the guiding center approximation. They solve only the equation of motion parallel to the magnetic field. The effect of cross-field transport is taken into account by diffusion approximation with an anomalous diffusion coefficient. In our code, the impurity ion trajectories are directly followed by numerically solving the 3D equation of motion,

$$m_{\rm I}\frac{{\rm d}\mathbf{v}}{{\rm d}t} = Ze(\mathbf{E}+\mathbf{v}\times\mathbf{B}) + (\text{Coulomb collision}) + (\text{multi-step ionization process}), \quad (1)$$

where $m_{\rm I}$ is the mass and Z is the charge number of impurity ions, $\mathbf{E}$ and $\mathbf{B}$ are the electric field and the magnetic field, respectively. The modeling including Larmor motion is essential for the analysis of the prompt redeposition of impurity ions.

To simulate the friction force by the background plasma and also the energy relaxation process toward the background plasma temperature, we have taken into account the Coulomb collision by binary collision method (BCM) [13]. The velocity of a background hydrogen ion involved in the binary collision with a test impurity ion is sampled from a shifted Maxwellian velocity distribution with a given local plasma temperature $T_{\rm i}$ and with a given local flow velocity $V_{\parallel}^{\rm f}$ parallel to the magnetic field. Scattering angles (θ,ϕ) in the center of mass system in a small time step Δt are randomly chosen by the Monte Carlo Method. The angle θ is given by $\theta = 2\arctan\xi_2$ and a random number ξ_2 is chosen from the Gaussian distribution with the statistical average $\langle\xi_2\rangle = 0$ and the variance $\langle\xi_2^2\rangle = (Z^2e^4 n_{\rm i}\ln\Lambda/8\pi\varepsilon_0^2 m_{\rm r}u^3)\Delta t$, respectively. Here, $n_{\rm i}$ is the background ion density, $m_{\rm r}$ is the reduced mass, u is the relative velocity between the impurity and the background plasma ion. The angle ϕ is given by $\phi = 2\pi\xi_3$ with a uniform random number ξ_3. The remaining notations are the conventional ones. At present, parallel thermal forces by electrons and ions are taken into account by a relatively simple way as in Refs. [3,4]. The expression for the parallel thermal force by the fluid model [1] is used and $\alpha_z\nabla_\parallel T_{\rm e} + \beta_z\nabla_\parallel T_{\rm i}$ is simply added for each test particle. The expressions for the coefficients, α_z and β_z are given in Ref. [1]. However, as pointed out recently in Ref. [5], this approach tends to overestimate β_z, especially, in the cases where the relative velocity of test particles ($\mathbf{v} - V_{\parallel}^{\rm f}\mathbf{b}$, where $\mathbf{b} = \mathbf{B}/B$) is of the order of the background ion thermal velocity. The modeling for the kinetic thermal force will be incorporated in the future.

Multi-step ionization and recombination processes of impurity ions are taken into account in the code by implicit Monte Carlo (IMC) method [14]. The transition probability from the k'th charge state to the kth charge state after a time step Δt can be calculated from the system of rate equations for each charge state. The ionization and recombination rate coefficients in the rate equations are calculated for tungsten ions from the Ref. [11]. The transition probabilities are tabulated for each spatial cell with a given background electron temperature $T_{\rm e}$ and density profiles $n_{\rm e}$ prior to the numerical integration of Eq. (1). During each time step of the time integration, the transition of the impurity ion charge-state is determined from a random uniform number ξ_4 ($0 < \xi_4 \leqslant 1$). If $\sum_{i=0}^{k-1} P_{k'\to i}(\Delta t) \leqslant \xi_4 < \sum_{i=0}^{k} P_{k'\to i}(\Delta t)$, the charge number Z in Eq. (1) must be changed from $Z_{k'}$ to Z_k. The density of impurity ions with each charge state Z_k in each numerical cell can be obtained in the same manner as for the neutrals.

3. Initial results

For the purpose of the checking code, a relatively simple geometric model was used in the present study (Fig. 1). The prompt redeposition rate of sputtered tungsten particles was calculated. The prompt redeposition rate r is defined by $r = N_{\rm redep}/N_{\rm total}$ where $N_{\rm total}$ is the total number of sputtered particles and $N_{\rm redep}$ is the number of particles redeposited onto the plate during their first Larmor period after ionization. The critical parameter p for the prompt redeposition is the ratio of the mean free path $\lambda_{\rm ion}$ to the Larmor radius $\rho_{\rm L}$, i.e., $p = \lambda_{\rm ion}/\rho_{\rm L}$ [9,10]. The prompt redeposition rate depends strongly on the parameter p. If we assume that the angular distribution of sputtered neutrals is a cosine distribution, the rate r can be obtained analytically [9,10];

$$r = \frac{1}{2}\left[1 + \mathrm{sgn}(1-p)\left(1 + \frac{4p^2}{(1-p^2)^2}\right)^{-1/2}\right]. \quad (2)$$

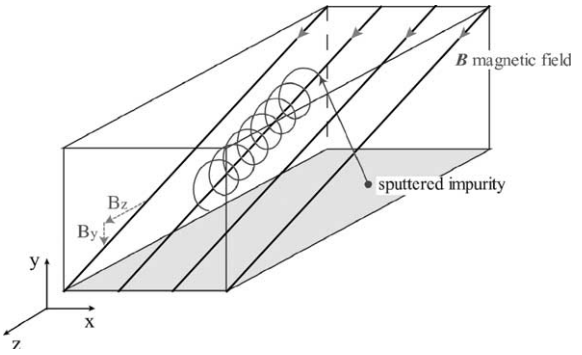

Fig. 1. Simple model geometry and coordinate system used in the analysis. The magnetic field lines are also shown. The B_z and B_y components correspond to the toroidal field and the poloidal field components, respectively.

In order to compare our code results with those calculated by this analytical expression, we first calculated a 'simplified case'. The magnetic field was fixed to be $B_z = 2T$ and $B_y/B_z = 0.05$ throughout the following calculation. On the other hand, in this simplified case, L_{ion} was varied to change the parameter p systematically and the L_{ion} was taken to be the same for all the neutrals for each value of L_{ion}. The neutrals were launched from a point source at $(x, y, z) = 0$ and the total number of 10^4 test flights was used in the calculation. The numerical results (open circles) are shown in Fig. 2 with the analytical results (solid line) obtained by Eq. (2).

In Fig. 2, we also show the numerical results (closed symbol) based on the model described in Section 2.1, i.e., the ionization length L_{ion} was randomly chosen by Monte Carlo method. The background electron plasma profiles of n_e and T_e were assumed to be uniform. They have been changed in the range of $n_e = 1$–5×10^{19} m^{-3} and $T_e = 5$–50 eV to vary the parameter p. The remaining conditions were the same as above. The prompt redeposition rates in this case (closed circles) become larger in comparison with those of the simplified case, especially for large p, since neutrals with short L_{ion} can contribute to the prompt deposition. In this case, we switched off the multi-step ionization process and the impurities were forced to be singly charged with $Z = 1$. If we take account of successive ionization, the prompt redeposition rate is reduced as shown in Fig. 2 (closed squares) particularly for small p. This is mainly due to a smaller Larmor radius with $Z = 2$ as pointed out in Ref. [10]. The comparison of the trajectories with multi-step ionization and without the multi-step ionization is shown in Fig. 3(a) and (b) for the same value of p ($p = 0.84$). The reduction in orbit radius by ionization to a higher charge state is clearly seen in Fig. 3(b). For this small p case with relatively large $T_e = 15$ eV and $n_e = 3 \times 10^{19}$ m^{-3}, the ionization time to higher charge states possibly becomes smaller than the first gyro period. The effect of Coulomb collisions on the prompt redeposition is relatively small, because the momentum and energy relaxation time are larger compared with the first gyro period. As was described in Section 2, we have employed the IMC method [14] for the atomic process. The IMC method is free from the condition $\Delta t \ll \tau^{\text{i/r}}$, where Δt is the numerical time step and $\tau^{\text{i/r}}$ is the characteristic time of the ionization/recombination. Thus, in the present numerical simulations, Δt has been determined so as to satisfy the condition $\Delta t \ll \tau^{\min}$ ($\Delta t = 0.01\tau^{\min}$) at each time step, where $\tau^{\min}$ has been chosen from the least value between the Larmor period and the slowing down time by Coulomb collision with background ions. Once the time step is changed, then transition probabilities $P_{k' \to k}(\Delta t)$ are recalculated.

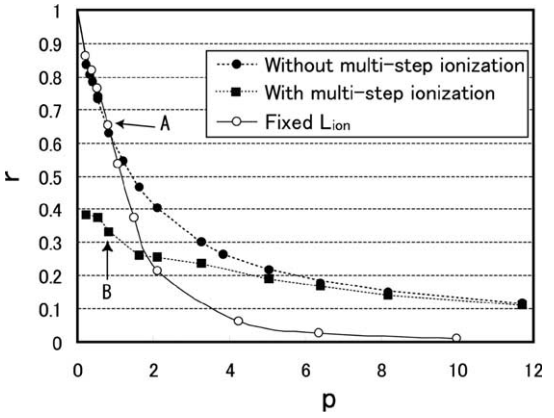

Fig. 2. Prompt redeposition rate r and its dependence on the parameter p ($= L_{\text{ion}}/\rho_L$).

In a detached plasma, the plasma temperature in front of the target plate becomes low, typically less than 5 eV. As a result, the ionization front moves upstream away from the target plate. The peak of the electron density also tends to be at a position removed from the plate. In this case, the parameter p becomes larger and the effect of prompt redeposition is reduced.

To study systematically the heavy metal impurity behavior in such detached plasmas, simple model calculations have just started. The slab geometry shown in Fig. 1 was used. The z-direction corresponds to a toroidal direction, the y-direction to a poloidal direction, and the x-direction to a radial direction. The boundaries in the y-direction ($y = 0$ m and $y = 0.1$ m) correspond to the target plate and the divertor entrance, respectively. By assuming toroidal symmetry ($\partial/\partial z = 0$), the impurity density profiles in the poloidal cross-section were calculated. The assumed background plasma profiles in the y-direction for $n_e(y)$, $T_e(y)$ and $V_{\parallel}^{\text{f}}(y)$ are shown in Fig. 4, while they were set to be uniform in the x-direction. The results are shown in Fig. 5. All the effects described in Section 2.2, except for the electric field in the pre-sheath

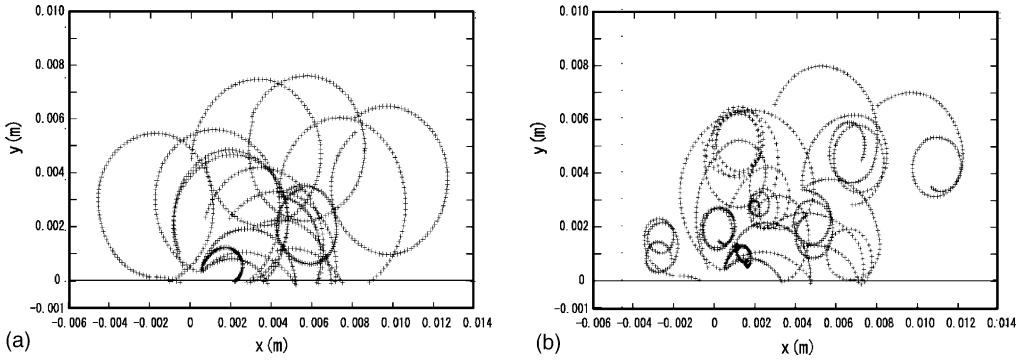

Fig. 3. Comparison of the trajectories (a) without multi-step ionization and (b) with the multi-step ionization. These trajectories are obtained for the point 'A' and 'B' in Fig. 2 with the same value of p ($p = 0.84$). The trajectories are projected to the (x, y) plane.

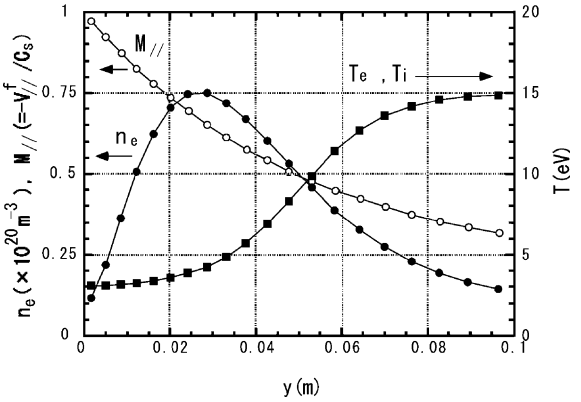

Fig. 4. Background plasma profiles of the electron density n_e, the electron temperature T_e and the parallel flow velocity $V_\parallel^f$ toward the plate. The ion density and temperature are assumed to be the same as those for electrons ($n_i = n_e$, $T_i = T_e$). The flow velocity $V_\parallel^f$ is normalized by the ion sound speed C_s.

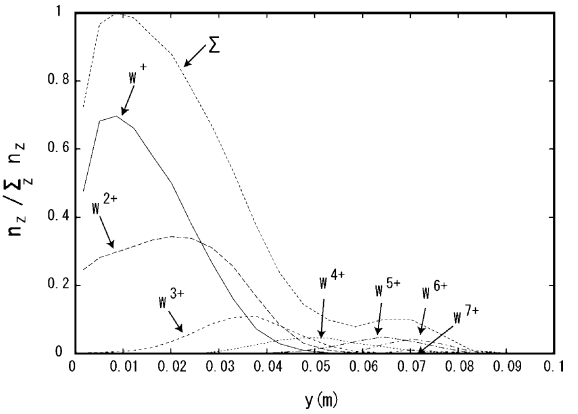

Fig. 5. Normalized density profiles for each charge state of tungsten. The 2D profiles are first averaged over in the x-direction and the resultant x-averaged densities $\bar{n}_z(y)$ are normalized to the maximum of the total impurity density $[\Sigma_z \bar{n}_z(y)]_{max}$. The profile of the normalized total impurity density $\Sigma_z \bar{n}_z(y)/[\Sigma_z \bar{n}_z(y)]_{max}$ is also shown by a dotted line with Σ.

and the sheath region, were taken into account for the impurity ion transport. The initial energy E_0 of sputtered particles is randomly chosen by a Monte Carlo method from the following energy distribution function, $S(E_0) = S_0(E_0/U_0^2)\exp(-E_0/U_0)$ with S_0 being the normalization factor and $U_0 = 8.66$ eV as in Ref. [2]. The angular distribution was assumed to be a cosine distribution. Only the source at the plate was considered. Their source strength was assumed to be uniform along the plate. The other boundaries ($x = \pm 0.1$ m, and $y = 0.1$ m) were taken as complete absorption boundaries. In Fig. 5, the parameter p at the target plate becomes very large $p = 123$, since T_e ($= 3$ eV) and n_e ($= 1.2 \times 10^{19}$ m^{-3}) are low at the target plate as shown in Fig. 4. Thus, the prompt redeposition rate becomes very small ($r = 1.9 \times 10^{-2}$) in this simulation, as was expected. However, Fig. 5 shows a favorable result for a choice of tungsten divertor in ITER, i.e., most of the tungsten particles sputtered from the target plate are retained in the divertor region ($y < 0.09$ m). To make more quantitative discussion and/or comparison with experiments, our code requires further development, e.g., inclusion of self-sputtering, the electric field and the kinetic thermal force. These initial results show the code has potential as a useful tool, not only for analysis of the prompt redeposition very close to the wall, but also for more large scale impurity transport even including the core region.

4. Future plan

The following items will be refined for further improvement of the code: (1) a relatively simple model has been used for both the generation process and the source profile of the impurity, especially, inclusion of the self-sputtering process is important, (2) the effect of electric

field in the pre-sheath and the sheath region must be taken into account, (3) the modeling for the kinetic thermal force will be incorporated, (4) including the anomalous cross-field diffusion process, (5) taking into account a more realistic tokamak geometry which includes SOL and core plasma regions, and (6) comparison with experiments will be needed for more quantitative and detailed code validation.

Acknowledgements

The authors are grateful to Drs Takizuka, K. Shimizu, Y. Tomita and Professor emeritus T. Amano at NIFS for fruitful discussion.

References

[1] J. Neuhauzer, W. Schneider, R. Wunderlich, et al., Nucl. Fusion 24 (1984) 39.
[2] S. Sengoku, M. Azumi, Y. Matsumoto, et al., Nucl. Fusion 19 (1979) 1327.
[3] P.C. Stangeby, C. Farrel, C. Hoskins, et al., Nucl. Fusion 28 (1988) 1945.
[4] K. Shimizu, H. Kubo, T. Takizuka, et al., J. Nucl. Mater. 220–222 (1995) 410.
[5] R. Reiser, D. Reiter, M.Z. Tokar, Nucl. Fusion 38 (1998) 165.
[6] J.N. Brooks, Nucl. Technol. Fusion 4 (1983) 33.
[7] D. Naujoks, R. Behrisch, J.P. Coad, et al., Nucl. Fusion 33 (1993) 581.
[8] K. Ohya, R. Kawakami, T. Tanabe, et al., J. Nucl. Mater. 290–293 (2001) 303.
[9] G. Fussman et al., in: Proceedings of the 15th International Conference of Plasma Physics and Controlled Nuclear Fusion Research, IAEA, Viena, vol. 2, 1995, p. 143.
[10] D. Naujoks, K. Asmussen, M. Bessenrodt-Weberpals, et al., Nucl. Fusion 36 (1996) 671.
[11] K. Asmussen et al., Nucl. Fusion 38 (1998) 967.
[12] M.H. Hughes, D.E. Post, J. Comp. Phys. 28 (1977) 43.
[13] T. Takizuka, H. Abe, J. Comp. Phys. 25 (1977) 205.
[14] A. Suzuki, T. Takizuka, K. Shimizu, et al., J. Comp. Phys. 131 (1997) 193.